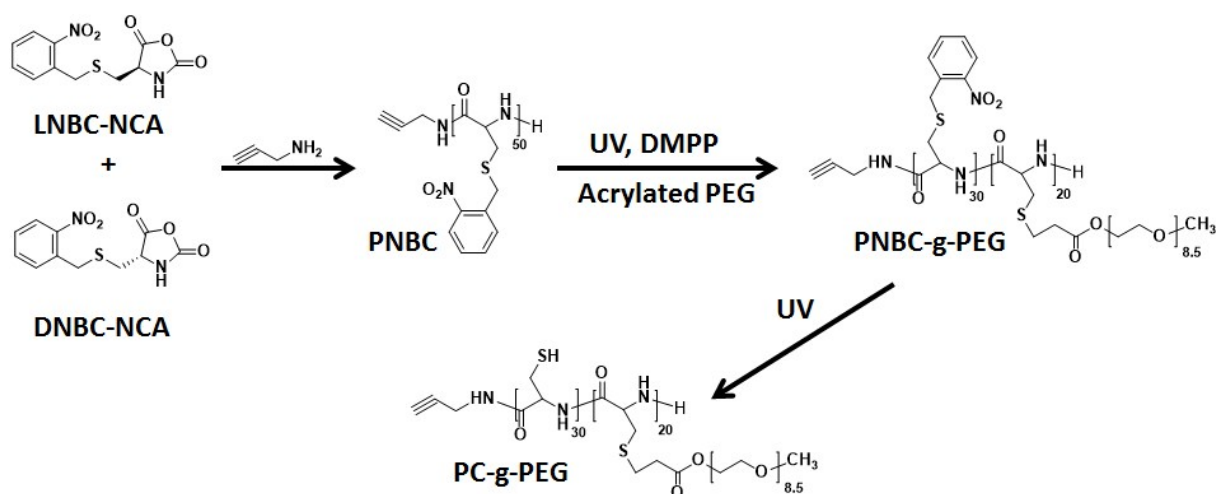


Supporting Information

An Autoreduction Method to Prepare Plasmonic Gold-Embedded Polypeptide Micelles for Synergistic Chemo-Photothermal Therapy

Xingjie Wu, Linzhu Zhou, Yue Su, Chang-Ming Dong*



Scheme S1. Synthesis of PNBC and the related graft copolymers PNBC-g-PEG and PC-g-PEG. Note: the photocleavage reaction of PNBC-g-PEG into PC-g-PEG was monitored by UV-vis spectroscopy and the chemical structures of both PNBC-g-PEG and PC-g-PEG were characterized by ^1H NMR and GPC (**Figure S1**).

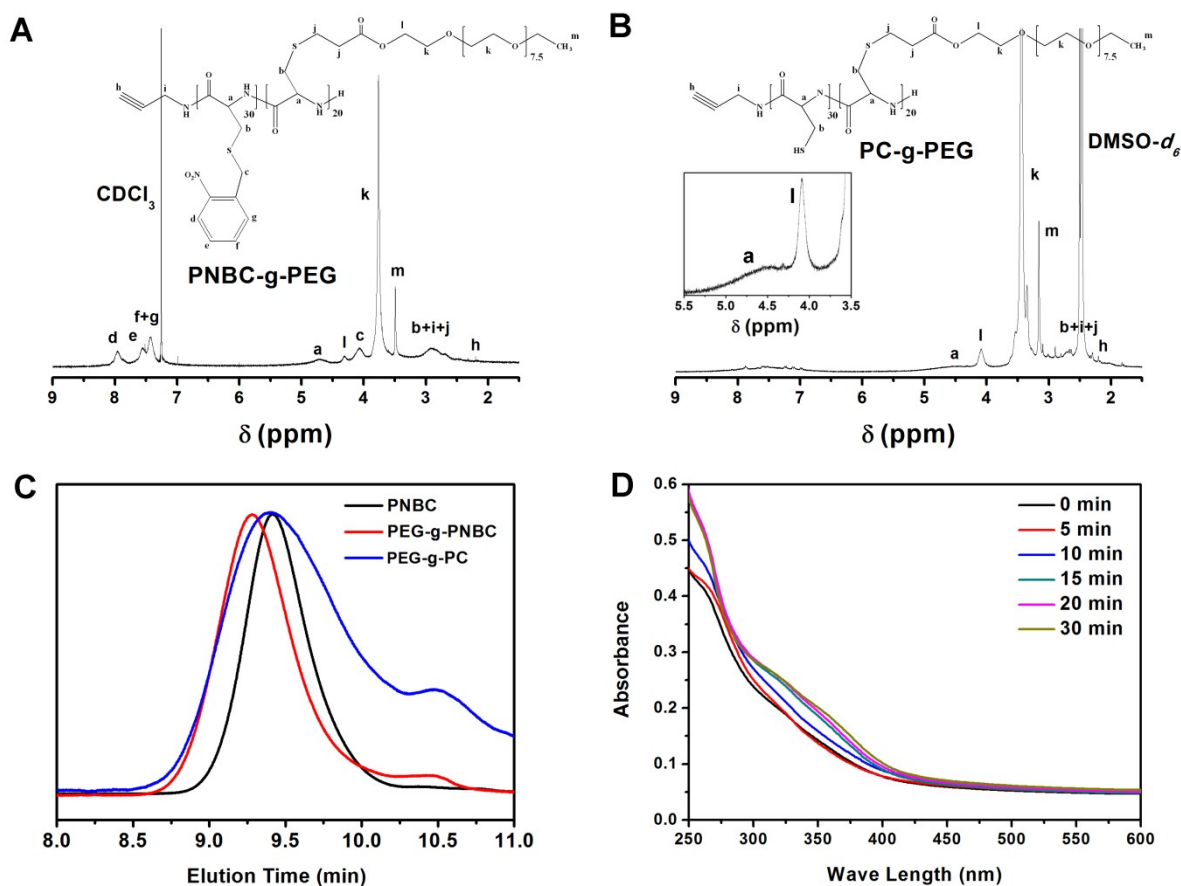


Figure S1. ^1H NMR spectra of PNBC-g-PEG (A) and PC-g-PEG (B); (C) the GPC traces for the precursor PNBC and the polypeptide graft copolymers; (D) UV-vis spectra for monitoring the photocleavage of PNBC-g-PEG (0.5 mg/mL) into PC-g-PEG upon different times of 365 nm UV irradiation. Note: PC-g-PEG contains multiple pendant thiols along the PC backbone, which could induce the intra-/inter-molecular cross-linking and strong interactions with GPC columns. Thus PC-g-PEG presented a broad polydispersity and a shoulder peak in GPC curve compared with its precursor PNBC-g-PEG.

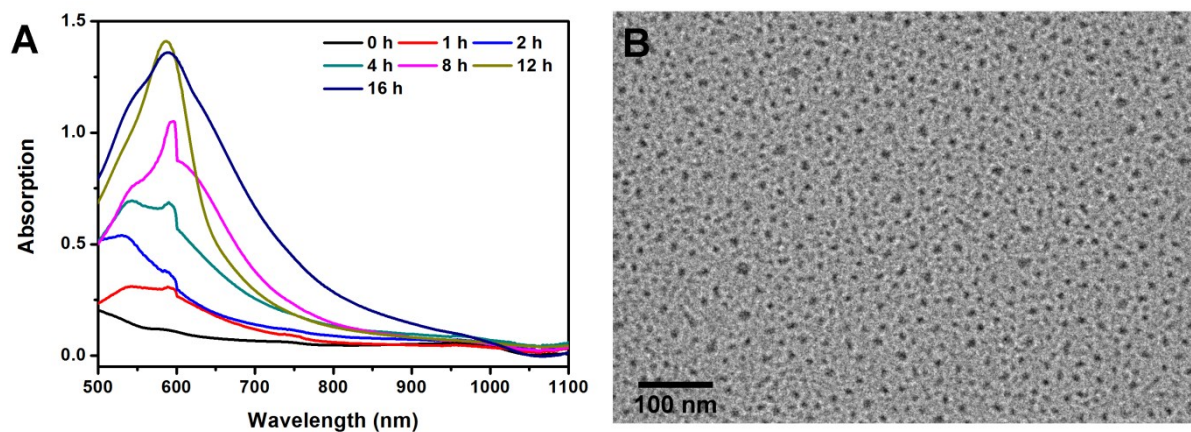


Figure S2. (A) Vis-NIR spectra for monitoring the reaction kinetics and TEM photograph (B) of the small gold nanoparticles tethered by PC-g-PEG (i.e., PC-g-PEG@Au NPs) in aqueous solution.

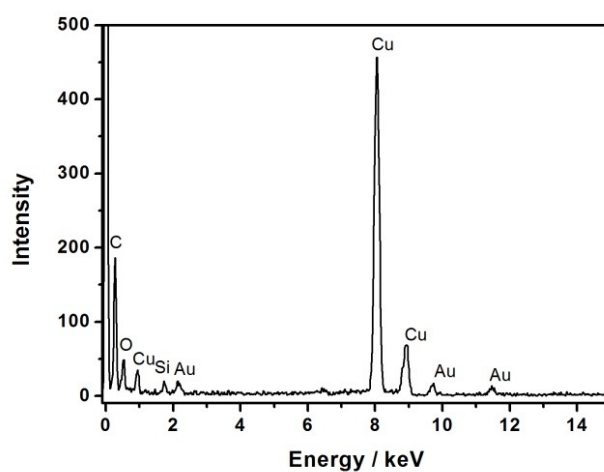


Figure S3. The energy dispersive spectroscopy of the gold-embedded micelles.

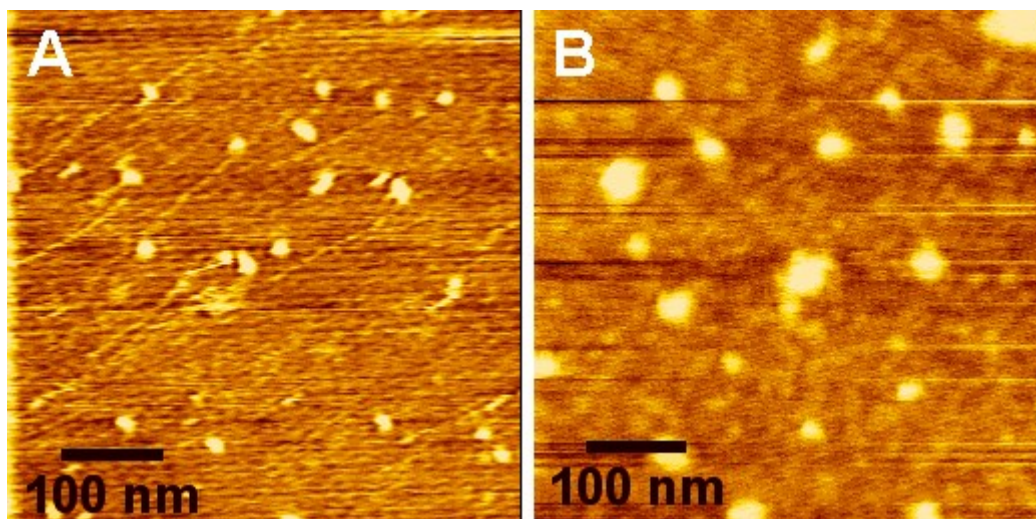


Figure S4. The phase images of AFM for the precursor micelles of CR Micelle (A) and the gold-embedded micelles of CR Micelle@30 μL .

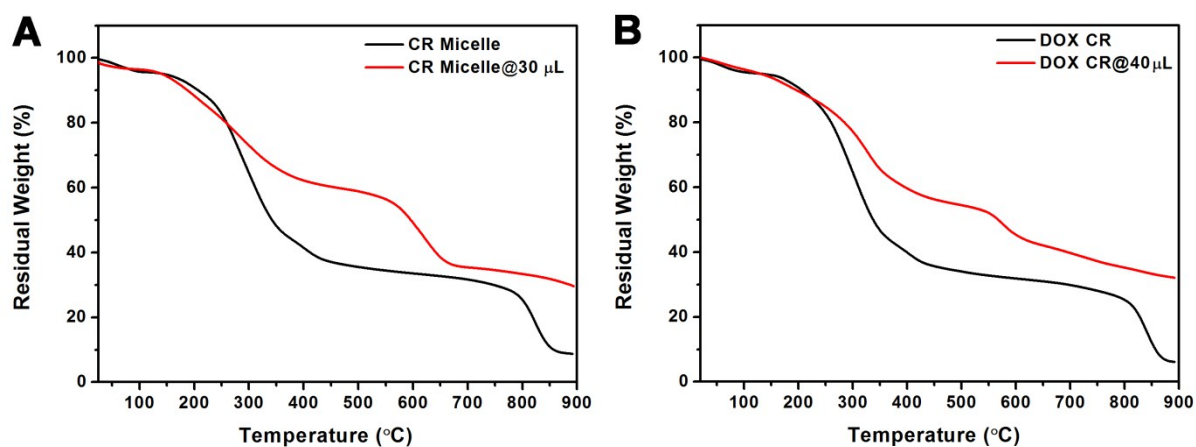


Figure S5. TGA curves for the precursor micelles and the gold-embedded micelles (A) and the DOX-loaded micelles and the DOX-loaded hybrid micelles (B).

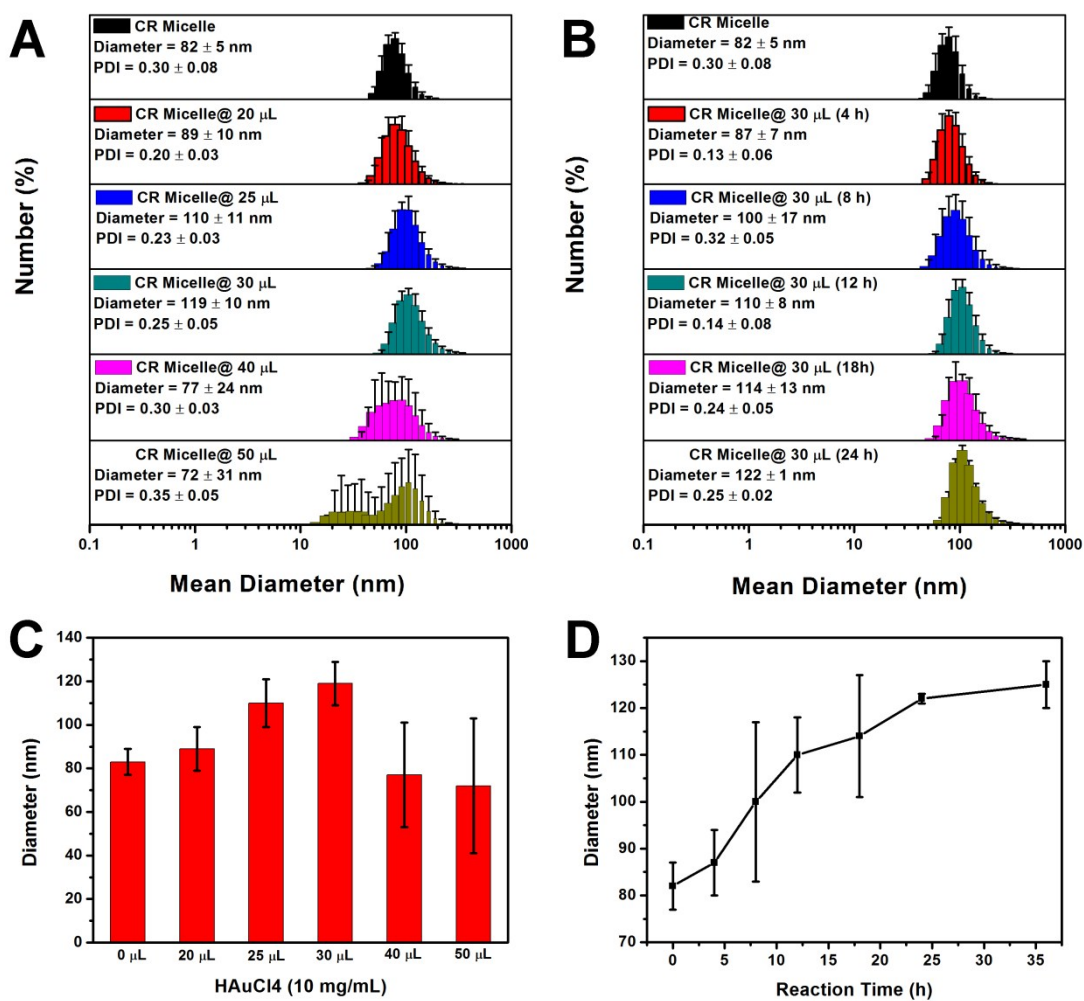


Figure S6. (A, C) DLS data for the cross-linked (CR) micelles and the resulting gold-embedded micelles with different amounts of HAuCl₄ (20, 25, 30, 40, 50 μL) (i.e., CR Micelle@20μL...); (B, D) DLS data for monitoring the reaction kinetics of the gold-embedded micelles with addition of 30μL HAuCl₄ (i.e., CR Micelle@30μL).

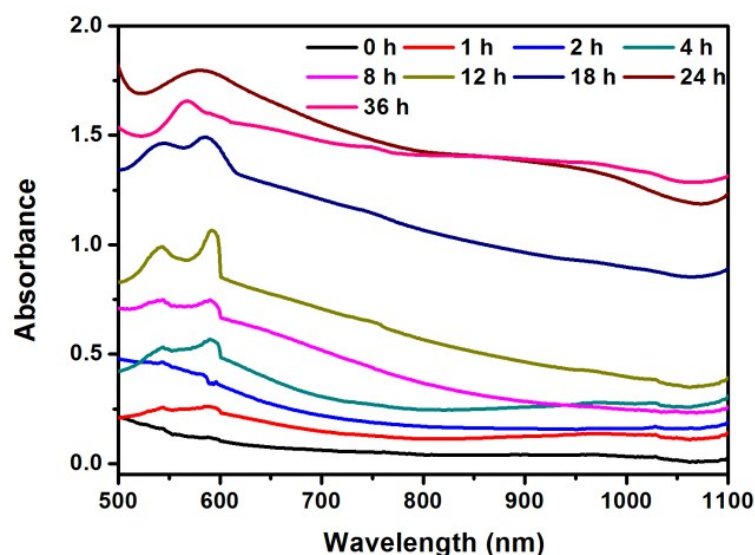


Figure S7. Vis-NIR spectra for monitoring the reaction kinetics of the gold-embedded micelles with addition of 30 μ L HAuCl₄ (i.e., CR Micelle@30 μ L).

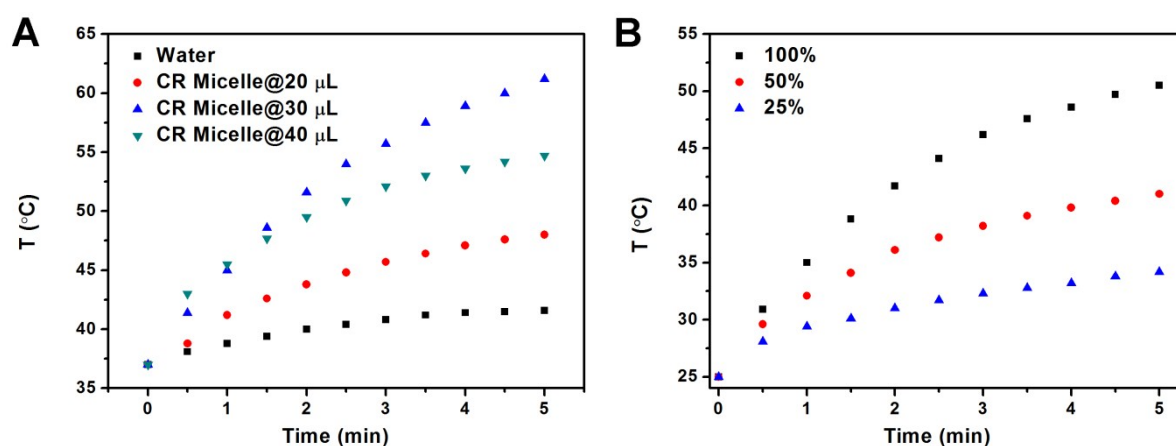


Figure S8. (A) The heating curves of the gold-embedded micelles solution upon NIR laser irradiation as a function of irradiation time (starting from 37 $^{\circ}$ C); and (B) the heating curves of different concentrations of the gold-embedded micelles solution (CR micelle@30 μ L: 0.48 mg/mL, 100%; 0.24 mg/mL, 50%; and 0.12 mg/mL, 25%) upon NIR laser irradiation as a function of irradiation time.

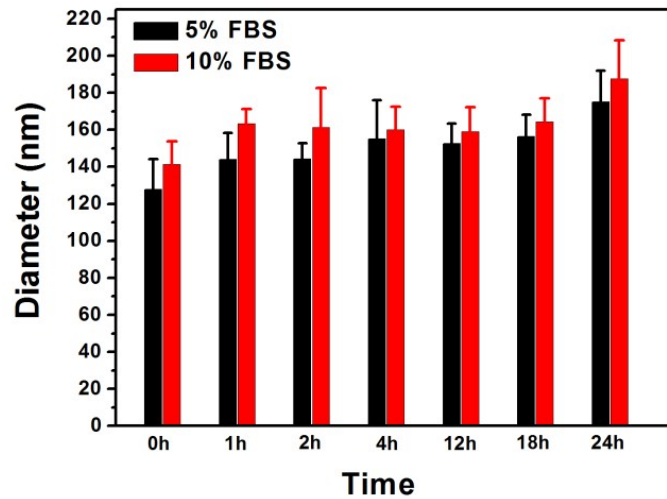


Figure S9. The size dependence of the gold-embedded micelles (0.12 mg/mL) on incubation time in the presence of different concentration of FBS at 37 °C.

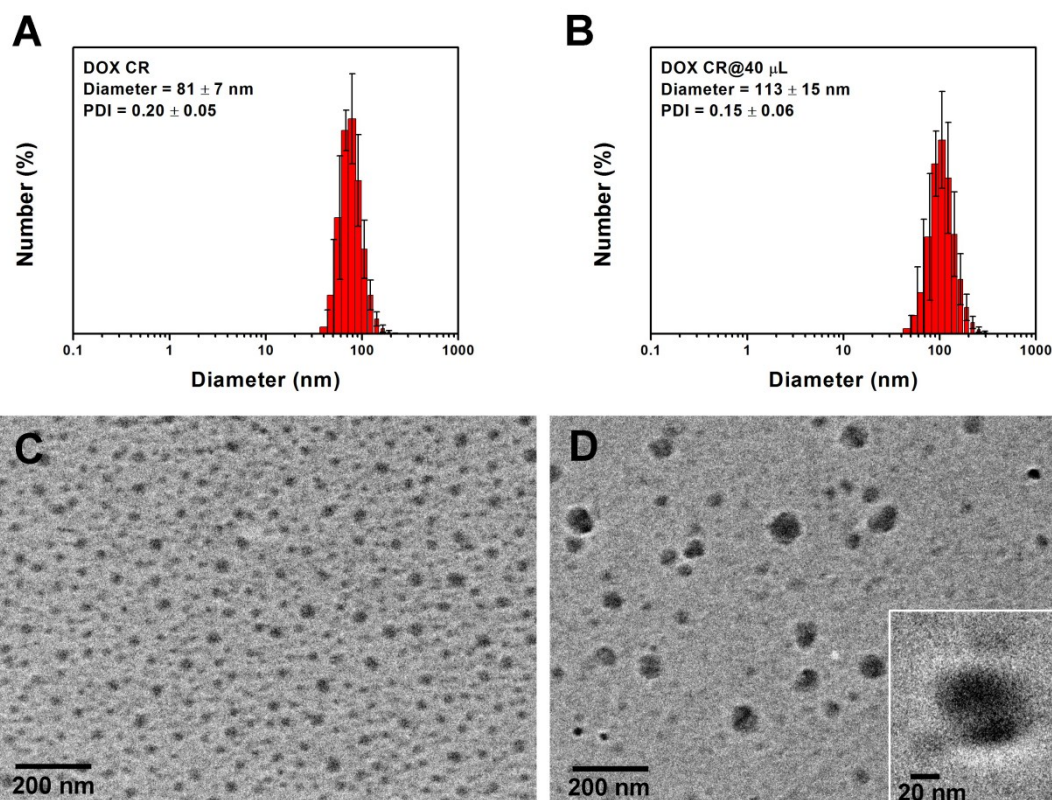


Figure S10. DLS and TEM data for the DOX-loaded disulfide-bond-cross-linked micelles (A, C) and the DOX-loaded and gold-embedded micelles (B, D).

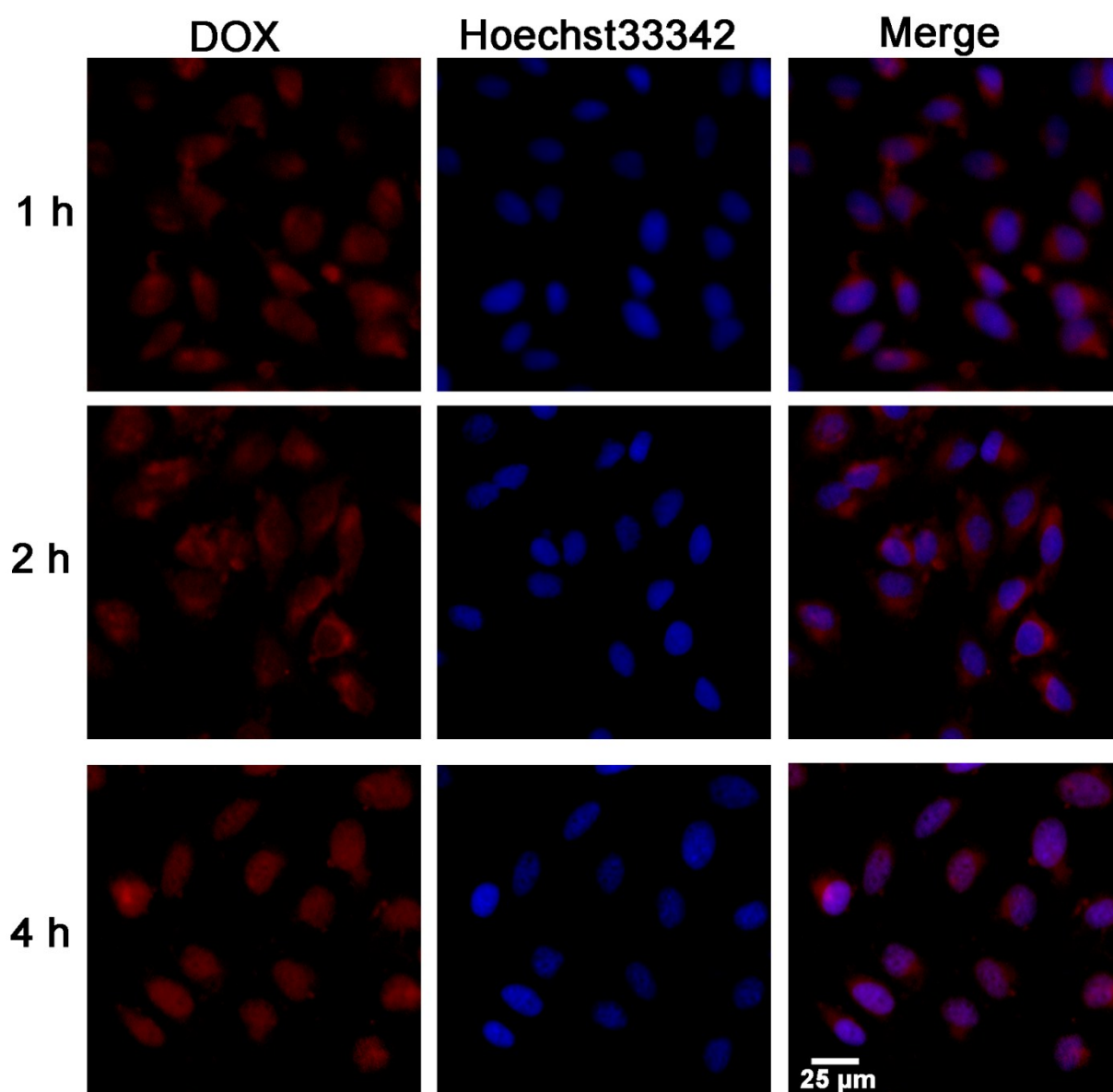


Figure S11. Fluorescence microscope images of HeLa cells incubated with the DOX-loaded and gold-embedded micelles at 1 h, 2 h and 4 h, respectively.

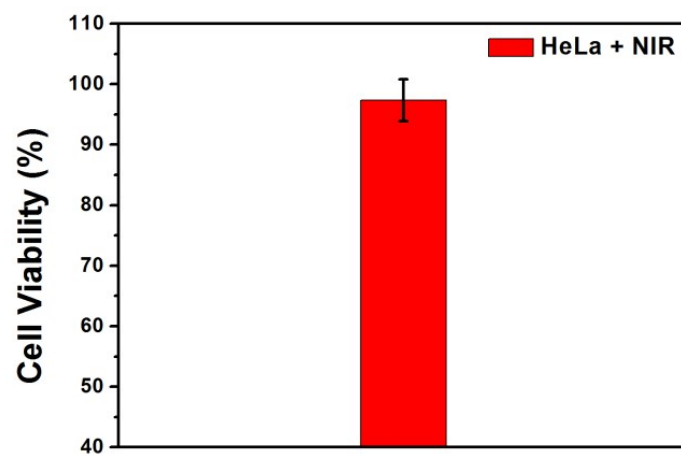


Figure S12. The cytotoxicity of laser irradiation (5 min, 808 nm, 2 W·cm⁻²) on HeLa cells. The cell viability was > 95%, which means that the NIR light irradiation nearly induced no cytotoxicity.